Joseph J. Thalakkottor
Department of Mechanical and
Aerospace Engineering,
University of Florida,
Gainesville, FL 32611
e-mail: tjjoseph@ufl.edu

Kamran Mohseni[1]
Department of Mechanical and
Aerospace Engineering;
Department of Electrical and
Computer Engineering,
University of Florida,
Gainesville, FL 32611
e-mail: mohseni@ufl.edu

Effect of Slip on Circulation Inside a Droplet

Internal recirculation in a moving droplet, enforced by the presence of fluid–fluid interfaces, plays an important role in several droplet-based microfluidic devices as it could enhance mixing, heat transfer, and chemical reaction. The effect of slip on droplet circulation is studied for two canonical steady-state problems: two-phase Couette, boundary-driven, and Poiseuille, pressure/body force-driven, flows. A simple model is established to estimate the circulation in a droplet and capture the effect of slip and aspect ratio on the droplet circulation. The circulation in a droplet is shown to decrease with increasing slip length in the case of a boundary-driven flow, while for a body force-driven flow it is independent of slip length. Scaling parameters for circulation and slip length are identified from the circulation model. The model is validated using continuum and molecular dynamics (MD) simulations. The effect of slip at the fluid–fluid interface on circulation is also briefly discussed. The results suggest that active manipulation of velocity slip, e.g., through actuation of hydrophobicity, could be employed to control droplet circulation and consequently its mixing rate. [DOI: 10.1115/1.4030915]

1 Introduction

Flow in a microchannel is often in low Reynolds transport region and, hence, inherently laminar. As a result, diffusion is the primary mode of momentum and heat transport from the wall. However, the presence of a fluid–fluid interface forms a circulatory flow inside a droplet. Circulation in a droplet plays an important role in several droplet-based applications due to enhanced mixing, heat transfer, and chemical reaction that results from it. It has an increased impact at small scales where surface effects start to dominate, as seen in several microfluidic applications, such as lab-on-a-chip, microreactors, and digitized heat transfer. Circulation helps in improving the efficiency of miniature-sized bio/chemical analysis systems that use microfluidic devices, such as lab-on-a-chip or micrototal analysis systems [1–3]. Circulation also increases mass transfer, which enhances diffusive penetration and consequently increases the observed reaction rates in microreactors. Microreactor technology offers numerous potential benefits for the process industries [4–6]. In the case of digitized heat transfer, discrete microdroplets are used to "digitally" transfer heat away from the source [7,8]. Circulation in a droplet results in convection normal to the wall, improving the efficiency of the thermal management system. Some research groups have already demonstrated rapid mixing or reaction by means of shuttling a droplet in a microchannel [9] or transporting it through a winding microchannel [10]. Hence, identifying and studying the parameters that affect the internal recirculation in a droplet are of great importance to these applications. This also suggest that by active manipulation of surface phobicity, and consequently slip, one could control circulation of a droplet. Here, we look at the effect of slip on droplet circulation.

Although slip at the boundary is prevalent for single phase flows, it is negligibly small in most continuum and macroscale applications. However, in many micro- and/or nano-scale applications, the first breakdown of the continuum assumption often occurs at a solid boundary in the form of velocity slip. Navier was the first to present a slip boundary condition for liquids in steady flows [11]. His model said that the slip velocity at the boundary is proportional to the shear rate of fluid at the wall, with the proportionality constant being called the slip length. Later, Maxwell presented a slip model for rarefied gases [12]. Although it was for rarefied gases, it demonstrated the same dependence of slip velocity on shear rate as Navier. Thompson and Troian [13] were the first to show that slip length was not a constant for a given fluid–wall pair but rather a function of shear rate. Recently, Thalakkottor and Mohseni [14] extended Maxwell's slip model to unsteady flows and showed that slip velocity was not only a function of the shear rate but also the gradient of the shear rate. Slip at microscales has been investigated extensively for single phase fluids [15], but research has been limited for two-phase flows [16–18].

The presence of circulatory flow inside a droplet has been widely reported for continuum scale problems [8,19,20] and more recently even at nanoscales [17]. Koplik et al. [16] and Thompson and Robbins [18] studied the motion of a contact line using MD simulations and demonstrated the presence of circulatory flow in molecular-scale droplets but did not quantify the total circulation in the droplet nor study the effects of slip on the total droplet circulation. Here, the effect of slip on droplet circulation is studied for two canonical steady-state problems: Couette, boundary-driven, and Poiseuille, pressure/body force-driven, flows. It is seen that the occurrence of fluid slip at the wall results in a significant change in circulation for a boundary-driven flow, where circulation is shown to decrease with increasing slip length. But, for flow driven by a pressure/body force, the total circulation in a droplet is independent of slip length. In this paper, two simple models are established, which help estimate circulation in a droplet for these two types of flows. The model demonstrates the effect of slip length and the inverse dependence of circulation on droplet $\mathcal{AR}$. It also helps to identify scaling parameters for circulation and slip length. The model is validated using results from continuum and MD simulations. The effect of slip, at the fluid–fluid interface, on circulation in a droplet is also briefly discussed.

Details of the problem setup are specified in Sec. 2. In Secs. 3 and 4, the circulation model is derived for a boundary-driven and pressure/body force-driven flow, respectively. The results are discussed in Sec. 5.

2 Problem Setup

In order to study the effects of wall slip on circulation, a two-dimensional (2D) droplet moving in contact with a wall is considered. Canonical problems of Couette and Poiseuille flows

[1]Corresponding author.

Contributed by the Fluids Engineering Division of ASME for publication in the JOURNAL OF FLUIDS ENGINEERING. Manuscript received December 23, 2014; final manuscript received June 12, 2015; published online August 4, 2015. Assoc. Editor: John Abraham.

corresponding to boundary- and pressure/body force-driven flow are simulated. The problem consists of two immiscible fluids in a channel of height H, with periodic boundaries along the x- and z-directions. In the case of a Couette flow, top and bottom walls move in opposite directions with a velocity U. A force-driven Poiseuille flow [21] is simulated by applying a constant body force along the x-direction. As the domain is periodic in x, a constant pressure gradient cannot be applied to drive the flow. Schematics of the problem geometries are shown in Fig. 1.

Simulations were performed using an incompressible Navier–Stokes solver [22], based on the volume-of-fluid method to describe variable density two-phase flows. In this method, the Navier–Stokes equation is written as

$$\nabla \cdot \boldsymbol{u} = 0 \tag{1}$$

$$\rho\left(\frac{\partial \boldsymbol{u}}{\partial t} + \boldsymbol{u} \cdot \nabla \boldsymbol{u}\right) = -\nabla P + \nabla \cdot (2\mu \boldsymbol{D}) + \rho \boldsymbol{a} + \gamma \kappa \delta_s \boldsymbol{n} \tag{2}$$

$$\frac{\partial c}{\partial t} + \nabla \cdot (c\boldsymbol{u}) = 0 \tag{3}$$

Here, $\boldsymbol{u} = (u, v, w)$ is the fluid velocity, ρ is the fluid density, P is the fluid pressure, μ is the dynamic viscosity, $\boldsymbol{D}$ is the deformation tensor, and $\boldsymbol{a}$ is the constant driving force per unit mass. Also, δ_s is the Dirac distribution function, γ is the surface tension, and κ and $\boldsymbol{n}$ are the curvature and normal to the interface, respectively. For two-phase flow, the volume fraction, $c(x, y, t)$, enables the tracking of the position of the interface. The density and viscosity are defined as

$$\rho = c\rho_1 + (1 - c)\rho_2 \tag{4}$$

$$\mu = c\mu_1 + (1 - c)\mu_2 \tag{5}$$

where ρ_1, ρ_2 and μ_1, μ_2 are the densities and viscosities of the first and second fluids, respectively.

Studies were conducted for different problem parameters and were found to be consistent with the results presented for the following parameters. In the case of a Couette flow, the walls are driven by an equal and opposite velocity, $U = 0.5$, while the Poiseuille flow is driven by a constant force per unit mass, $a = 1$. The fluid chosen has a viscosity $\mu_1 = 0.2$, density $\rho_1 = 1$, and surface tension $\gamma = 1.0$. The viscosity and density ratio between the fluid that makes up the droplet and the surrounding fluid is $\mu_{12} = \mu_1/\mu_2 = 100$ and $\rho_{12} = \rho_1/\rho_2 = 100$. These are the parameters used for all the results unless it is explicitly specified. The parameters are scaled by the channel height, characteristic velocity of the flow, and the density of the fluid. As the focus of this paper is on studying the effects of slip at the wall on circulation, the fluid properties were chosen such that the effects of viscosity ratio, surface tension, and contact angle hysteresis are negligible. However, the circulation model has been verified, and results presented, for a wider range of viscosity ratios and interfacial tensions for the case of flow driven by pressure/body force.

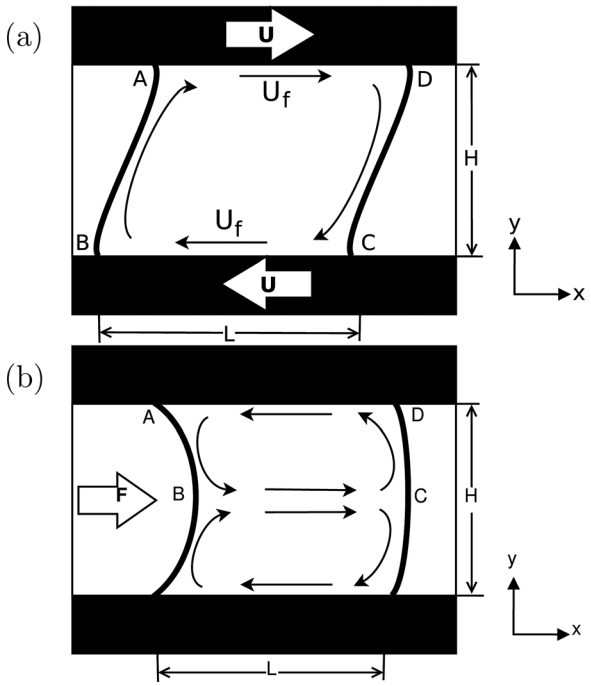

Fig. 1 Schematic of the problem of a 2D: (*a*) Couette flow and (*b*) body force-driven flow. The problem simulates a shear-driven and body force-driven flow with two immiscible fluids in a microchannel. Here, *z* is the out of plane axis.

MD simulations are used to study the variation of slip length along the wall. The MD simulations presented in this paper are performed using the LAMMPS package [23]. The fluid's initial state is modeled as a face-centered cubic (fcc) structure with the x-direction of the channel being aligned along the $[11\bar{2}]$ orientation of the fcc lattice. The wall comprises 2–3 layers of atoms oriented along the (111) plane of fcc lattice. The wall atoms are fixed to their lattice sites.

The pairwise interaction of molecules separated by a distance r is modeled by the Lennard–Jones (LJ) potential

$$V^{\mathrm{LJ}} = 4\varepsilon\left[\left(\frac{\sigma}{r}\right)^{12} - \left(\frac{\sigma}{r}\right)^{6}\right] \tag{6}$$

where ε and σ are the characteristic energy and length scales. The potential is zero for $r > r_c$, and the cutoff radius, r_c is 2.5σ.

The two different cases of wall–fluid properties used for MD are listed in Table 1.

3 Circulation Model for Boundary-Driven Flow

A mathematical model that describes the effect of slip length on circulation is established for a droplet moving in a 2D channel and it is then validated through direct continuum and MD simulations. The flow is driven by walls moving in opposite directions with a velocity, U, in the frame of reference of the droplet; see Fig. 1(*a*).

Velocity in the droplet is everywhere assumed to be equal to the Couette flow profile. Using the Navier slip boundary condition, the velocity of fluid adjacent to the wall can be written as

$$u_{\mathrm{f}}^{\mathrm{wall}} = U\left(\frac{H}{H + 2L_s}\right) \tag{7}$$

where L_s is the slip length. The top and bottom walls are assumed to have identical properties.

As the problem is symmetric, the circulation contribution by the top and bottom walls and the left and right interfaces is assumed to be the same. Hence, the total circulation inside a droplet is expressed as

Table 1 Different cases of wall–fluid properties are considered, with case 1 corresponding to a wetting (hydrophilic) wall and case 2 corresponding to a nonwetting (hydrophobic) wall

Case	$\epsilon^{\mathrm{wf}}/\epsilon$	$\sigma^{\mathrm{wf}}/\sigma$	ρ_w/ρ	L_s^o/σ
1 (wetting)	1.0	1.0	1	0.5
2 (nonwetting)	0.4	0.75	4	4.9

ϵ^{wf} and σ^{wf} are the LJ parameters for fluid–wall interaction, ρ_w/ρ is the relative density of wall, and L_s^o is the slip length calculated at the center of the droplet.

$$\Gamma = 2\int_0^{L} \boldsymbol{u}_{\mathrm{f}}^{\mathrm{wall}} \cdot \mathrm{d}\boldsymbol{l} + 2\int_0^{L_{\mathrm{int}}} \boldsymbol{u}_{\mathrm{f}}^{\mathrm{int}} \cdot \mathrm{d}\boldsymbol{l} \tag{8}$$

where L and L_{int} are the length of droplet along the wall and interface, respectively, and $\boldsymbol{u}_{\mathrm{f}}^{\mathrm{int}}$ is the fluid velocity along the fluid–fluid interface. The velocity of fluid along the interface is assumed to be $\boldsymbol{u}_{\mathrm{f}}^{\mathrm{int}} = k\boldsymbol{u}_{\mathrm{f}}^{\mathrm{wall}}$. Simulation results showed that the ratio of mean velocity along the interface to the velocity of fluid adjacent to the wall varies exponentially with slip length, that is, $k = a\exp(bL_s) + c\exp(dL_s)$. The fitting coefficients were found to be $a = 0.18$, $b = -10.42$, $c = 0.34$, and $d = -0.68$. Substituting the fluid velocity at the wall and performing a change of variable from $\mathrm{d}\boldsymbol{l}$ along the wall to x-direction and from $\mathrm{d}\boldsymbol{l}$ along the interface to y-direction, we obtain

$$\Gamma = 2\int_0^{L} U\left(\frac{H}{H + 2L_s(x)}\right)\mathrm{d}x + 2k\int_0^{H} \frac{U}{\sin\theta}\left(\frac{H}{H + 2L_s(y)}\right)\mathrm{d}y \tag{9}$$

where θ is the respective-averaged dynamic contact angle. Here, the averaged dynamic contact angle is defined as the acute angle formed by the wall and a straight line which describes the fluid–fluid interface. As the droplet is symmetric about the centerline, the left or right interface makes the same averaged dynamic contact angle. The dynamic contact angle is estimated from the "Hoffman–Voinov–Tanner" law, given as $\theta^3 = \theta_s^3 + 9\mathrm{Ca}\ln(\varepsilon^{-1})$ [24]. Here, θ_s is the static contact angle, Ca is the capillary number, and ε is a matching coefficient. The numerical coefficient multiplying the capillary number is found from the numerical results.

Slip length is assumed to be a constant along the wall, $L_s = L_s^o$, where L_s^o is the asymptotic value of slip length as defined in Ref. [13] for a single-phase Couette flow. By scaling x and y with L and H, respectively, and performing a change of variable, circulation along a droplet can be represented as

$$\frac{\Gamma}{UL} = \frac{2}{1 + 2\dfrac{L_s}{H}}\left(1 + \frac{k}{\mathcal{R}_\Gamma \sin\theta}\right) \tag{10}$$

Here, $\mathcal{R}_\Gamma$ is the aspect ratio of the vortex in the droplet, which for a boundary-driven flow is equal to the droplet aspect ratio, $\mathcal{R}$. In the case of Poiseuille flow which has two corotating vortices, $\mathcal{R}_\Gamma$ is twice that of the droplet $\mathcal{R}$. Writing the above equation in nondimensional form

$$\Gamma^* = \frac{2}{1 + 2L_s^*}\left(1 + \frac{k}{\mathcal{R}_\Gamma \sin\theta}\right) \tag{11}$$

where $\Gamma^* = \Gamma/UL$ and $L_s^* = L_s/H$. From the above expression, it can be seen that circulation varies inversely with slip length, though the extent of its effect on circulation is dependent on whether the length scale of the problem is comparable to the slip length scale. Also, it can be observed that for droplets with high $\mathcal{R}$, the contribution to circulation from the fluid–fluid interface reduces relative to the contribution from the wall.

4 Circulation Model for Pressure/Body Force-Driven Flow

A mathematical model that describes the effect of slip length on circulation is established for a droplet moving in a channel where the two fluids are immiscible. The flow is driven by a pressure gradient or a constant body force, in the lab frame of reference. A droplet driven by a constant body force exhibits two symmetric counter rotating flows; see Fig. 1(*b*). Model presented here estimates the total circulation of a single vortex, which extends from the wall to the droplet centerline. For a 2D, fully developed, steady-state single phase flow with Navier slip boundary condition at the wall, the axial velocity is given by

$$u = U\left(1 - \frac{4y^2}{H^2} + \frac{4L_s}{H}\right) \tag{12}$$

Here, $U = -(H^2/8\mu)(dp/dx)$ is the centerline velocity of a single-phase Poiseuille flow. If the flow is driven by a constant body force per unit volume, $\boldsymbol{f}$, instead of a pressure gradient, the centerline velocity will be $U = -(H^2/8\mu)\boldsymbol{f}$. The velocity profile in Eq. (12) can be interpreted as the superposition of a simple Poiseuille flow with no-slip boundary condition and a uniform flow of velocity, $4L_s/H$. The top and bottom walls are assumed to have identical properties.

Circulation in a control volume of length L and height $H/2$ is calculated as

$$\Gamma = \int_0^{L_c} \boldsymbol{u}_{\mathrm{f}}^{\mathrm{center}} \cdot \mathrm{d}\boldsymbol{l} - \int_0^{L_w} \boldsymbol{u}_{\mathrm{f}}^{\mathrm{wall}} \cdot \mathrm{d}\boldsymbol{l} + \int_0^{L_{l,\mathrm{int}}} \boldsymbol{u}_{\mathrm{f}}^{\mathrm{int}} \cdot \mathrm{d}\boldsymbol{l} + \int_0^{L_{r,\mathrm{int}}} \boldsymbol{u}_{\mathrm{f}}^{\mathrm{int}} \cdot \mathrm{d}\boldsymbol{l} \tag{13}$$

where L_c, L_w, $L_{l,\mathrm{int}}$, and $L_{r,\mathrm{int}}$ are the length of the vortex along the centerline, wall, left, and right interface, respectively. The velocity of fluid along the interface is assumed to be $\boldsymbol{u}_{\mathrm{f}}^{\mathrm{int}} = kU$, where k is a numerical constant [20]. This assumption is later verified in numerical simulations. Substituting the fluid velocity at the wall and performing a change of variable from $\mathrm{d}\boldsymbol{l}$ along the wall to x-direction and from $\mathrm{d}\boldsymbol{l}$ along the interface to y-direction, we obtain

$$\Gamma = \int_0^{L_c} U\left(1 + 4\frac{L_s(x)}{H}\right)\mathrm{d}\boldsymbol{x} - \int_0^{L_w} 4U\frac{L_s(x)}{H}\mathrm{d}\boldsymbol{x} + k\int_0^{H/2} \frac{U}{\sin\theta_l}\mathrm{d}\boldsymbol{y} + k\int_0^{H/2} \frac{U}{\sin\theta_r}\mathrm{d}\boldsymbol{y} \tag{14}$$

Here, θ_l and θ_r are the averaged dynamic contact angles at the left and right interfaces, which correspond to the trailing and leading contact angles. Similar to Sec. 3, the averaged dynamic contact angle is defined as the acute angle between the wall and a straight line which describes the fluid–fluid interface up to the center of the droplet. Scaling x and y with L and $H/2$, respectively, and performing a change of variable, circulation along a droplet can be written as

$$\frac{\Gamma}{UL} = 1 + 4\frac{L_s}{H}\frac{1}{\mathcal{R}_\Gamma}\left(\frac{1}{\tan\theta_r} - \frac{1}{\tan\theta_l}\right) + \frac{k}{\mathcal{R}_\Gamma}\left(\frac{1}{\sin\theta_r} + \frac{1}{\sin\theta_l}\right) \tag{15}$$

where $\mathcal{R}_\Gamma = L/(H/2)$ is the vortex aspect ratio, which is twice the droplet $\mathcal{R}$, defined based on droplet diameter, for a Poiseuille flow. Subscripts l and r refer to the left and right interfaces, respectively. This expanded form of the circulation model accounts for contact angle hysteresis.

By assuming no contact angle hysteresis, i.e., $\theta_r \approx \theta_l = \theta$, the model is simplified and one could obtain the nondimensional circulation to be

$$\frac{\Gamma}{UL} = 1 + \frac{2k}{\mathcal{R}_\Gamma \sin\theta} \tag{16}$$

Here, it is assumed that the difference in the droplet length, measured at the wall and the centerline, and the difference in the length of the two fluid–fluid interfaces in front and back of the droplet have a negligible affect on the total circulation of the droplet. The model is in agreement with that found in Ref. [20], where they experimentally investigate a moving droplet in an axisymmetric microtube, with no-slip boundary condition at the wall. While the

focus of their paper was on studying the effects of $\mathcal{AR}$ on the flow invariants in a droplet, we were able to use their data to validate our model. Using numerical results it is found that $k = 0.09$ for the cases considered in this study. This is consistent with the k values reported in Ref. [20], for different droplet aspect ratios.

It is known that the mean velocity of a droplet and consequently the centerline velocity, $\tilde{U}$, is lower than that of single phase fluid, U, subjected to the same driving force [25]. This is due to the addition of capillary pressure on top of the applied pressure gradient. The curvature of an interface leads to a pressure drop across the interface, described by the Young–Laplace equation [26,27]. The change in pressure gradient experienced by the droplet is then determined by the length of the droplet. Hence, an increase in the droplet $\mathcal{AR}$ results in a decrease in the effective pressure gradient due to the addition of the capillary pressure. There are several models that predict the net force applied on the droplet or the effective droplet velocity [25]. A generalized model based on Fuerstman et al. [28] and Baird and Mohseni's [29] models is used. It says that the pressure difference across a channel is given as

$$\Delta P = A\frac{\tilde{U}}{H^2}[\mu_1 L_1 + \mu_2 L_2] + \gamma(\cos\theta_r - \cos\theta_a) \tag{17}$$

where A is a numerical coefficient, $\tilde{U}$ is the centerline velocity in the middle of the droplet, H is the height of the channel, μ_1 and L_1 are the dynamic viscosity and length of fluid 1 (droplet), μ_2 and L_2 are the dynamic viscosity and length of fluid 2, γ is the surface tension, and θ_r and θ_a are the receding and ascending contact angles. Updating the circulation model using $\tilde{U}$ and rewriting it in nondimensional form, one obtains

$$\Gamma^* = 1 + \frac{2k}{\mathcal{AR}_\Gamma \sin\theta} \tag{18}$$

where $\Gamma^* = \Gamma/\tilde{U}L$. The total circulation in a pressure-driven droplet is seen to be independent of the slip length at the wall. Similar to boundary-driven flows, it is observed that for droplets with high $\mathcal{AR}$, the contribution to circulation from the fluid–fluid interface reduces relative to the contribution from the wall. The change in interface curvature or capillary forces due to slip (as it changes static contact angle), which results in a change in the total droplet circulation, is not captured in this model. This simple model could help in estimating the total circulation for a droplet using a priori known flow parameters.

5 Numerical Results

In Secs. 3 and 4, we developed a model for estimating circulation in a droplet driven by pressure/body forces or driven by the boundary. In this section, we conduct direct numerical simulations to verify the assumptions made and models derived. The various droplet sizes investigated are listed in Table 2. In addition, the effect of slip at the fluid–fluid interface is also briefly discussed.

Table 2 The aspect ratios of vortex in a droplet are presented

$\mathcal{AR}_\Gamma$	$\mathcal{AR}_\Gamma$ Couette	$\mathcal{AR}_\Gamma$ Poiseuille
1	0.91	0.98
3	—	2.91
4	3.72	—
7	6.67	6.75
10	9.52	9.63

In the paper, for clarity, the approximate aspect ratio, $\mathcal{AR}_\Gamma$, is mentioned but the exact aspect ratios used in this study are listed for a boundary-driven (Couette) and pressure/body force-driven (Poiseuille) flow problems. For a boundary-driven (Couette) flow, $\mathcal{AR}_\Gamma = \mathcal{AR}$, while for a pressure/body force-driven (Poiseuille) flow $\mathcal{AR}_\Gamma = 2\mathcal{AR}$, where $\mathcal{AR}$ is the droplet aspect ratio.

5.1 Boundary-Driven Flow. For the boundary-driven flow considered here, wall movement drives the circulation inside a droplet. Hence, it is intuitive that the occurrence of velocity slip at the wall, which impedes the transfer of momentum across the wall–fluid interface, will affect circulation. A change in circulation directly impacts the rate of mixing, mass and heat transfer, and chemical reaction, essential for various droplet-based microfluidic devices.

Figure 2(*a*) shows the variation of circulation with slip length for different droplet aspect ratios. It is observed that circulation decreases with increase in slip length at the wall, which is a measure of slip at the wall–fluid interface. For the limiting case of infinite slip (perfect slip) at the wall, circulation reduces to zero. The total droplet circulation is also seen to increase with the droplet $\mathcal{AR}$. These are consistent with the circulation model developed in Eq. (11). Plotting the nondimensional values of circulation and slip length shows the collapse of data onto a single curve; see Fig. 2(*b*). When the slip length is comparable to the height of the droplet, it has a significant affect on the total droplet circulation. Slip lengths of the order of 10 μm [30,31] have been reported in the literature for water on a superhydrophobic surface which is comparable to the length scale of several micro/nano-fluidic devices. In such a case, the total circulation could be significantly affected.

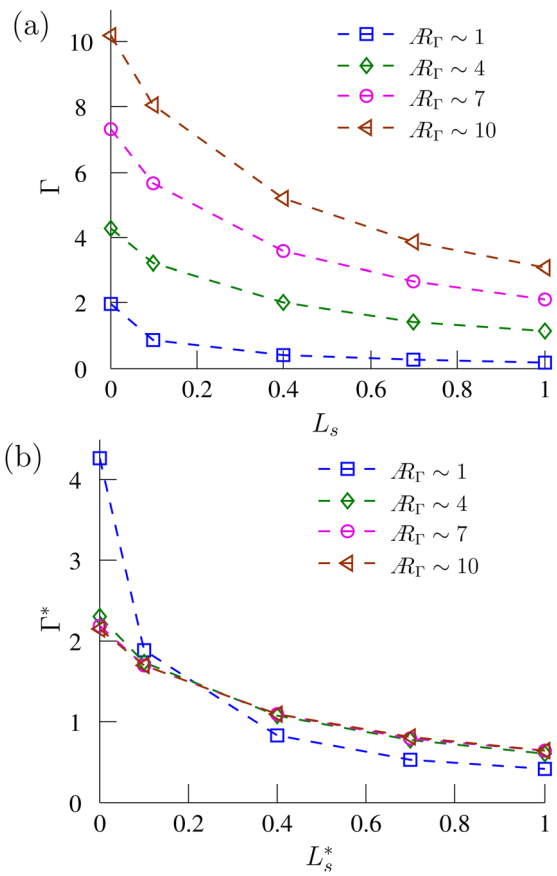

Fig. 2 Circulation versus slip length for droplets with different $\mathcal{AR}_\Gamma$. Here, vortex aspect ratios equals the droplet aspect ratio, $\mathcal{AR}_\Gamma = \mathcal{AR}$. (*a*) The unscaled data and (*b*) the scaled. Results from continuum simulations show the decrease in circulation with increasing slip length and decreasing vortex $\mathcal{AR}$. The scaled results for different droplet $\mathcal{AR}$ collapse, except for $\mathcal{AR}_\Gamma = 1$. Here, $\Gamma^* = \Gamma/UL$, $L_s^* = L_s/H$.

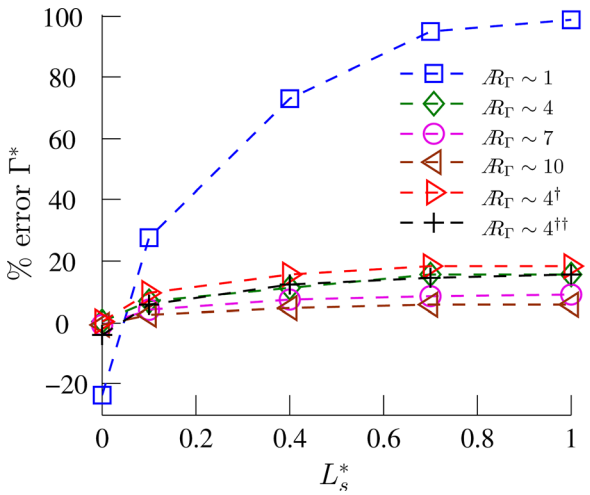

Fig. 3 Percentage error of nondimensional droplet circulation in continuum simulations. The error is computed as $(\Gamma^*_{\text{model}} - \Gamma^*_{\text{simulation}})/\Gamma^*_{\text{simulation}}$, where $\Gamma^* = \Gamma/UL$. The error increases with decrease in droplet $\mathcal{AR}$ and an increase in slip length. Unless specified, the parameters for different cases were (surface tension) $\gamma = 1$, (static contact angle) $\theta_s = 90$ deg, and (viscosity ratio) $\mu_{12} = 100$. For high $\mathcal{AR}$, the relative error is less than 20%. Here, † is $\Gamma = 0.6$, $\theta = 120$, and †† is $\mu_{12} = 50$.

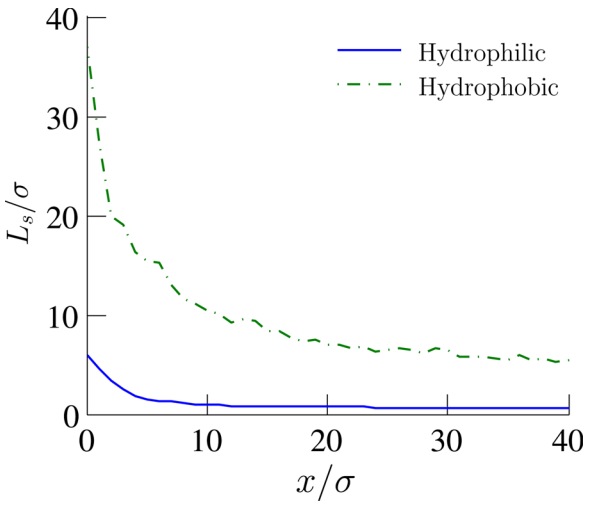

Fig. 4 Variation of slip length on the wall while moving away from the TCP. Two cases with hydrophilic and hydrophobic wall are shown. The results are obtained using MD simulations, where σ is the LJ parameter corresponding to the diameter of the molecule and having units of an Å. The details of the two cases are listed in Table 1.

For the case of a boundary-driven flow, aspect ratio of the vortex equals the droplet aspect ratio, $\mathcal{AR}_\Gamma = \mathcal{AR}$. The circulation model in Eq. (11) shows that the contribution of circulation from the fluid–fluid interface varies as $\mathcal{AR}^{-1}$. Hence, for a droplet with large $\mathcal{AR}$, the contribution to total circulation from the fluid–fluid interface is negligible as compared to that of the wall.

The accuracy of the circulation model, developed in Sec. 3, is evaluated by comparing it with simulation results for a boundary-driven flow with varying droplet aspect ratios; see Fig. 3. The relative error is plotted against the slip length, for droplets with different aspect ratios, $\mathcal{AR}$, surface tension, γ, and viscosity ratio, μ_{12}. The relative error is calculated as $(\Gamma^*_{\text{model}} - \Gamma^*_{\text{simulation}})/\Gamma^*_{\text{simulation}}$. For droplets with large $\mathcal{AR}$, the maximum relative error is bounded to 20%. However, for most practical applications, the slip length will be orders of magnitude smaller than the length scale of the droplet, for which case, the relative error reduces to less than 10%. We believe the two main sources of error in the model are the assumptions of constant slip length along the wall and the assumption of a linear axial velocity profile throughout the droplet. These are discussed below.

First, we investigate the validity of the assumption of constant slip length along the wall. For a given $\mathcal{AR}$, the relative error is observed to increase with slip length and reach an asymptotic value at higher magnitudes of slip length; see Fig. 3. In Fig. 4, variation of slip length along the wall is shown as the distance from the triple contact point (TCP), for a hydrophilic and a hydrophobic wall. The results are presented from MD simulations. In the vicinity of the TCP, there is a sharp increase in the slip length from its asymptotic value, L_s^o, which is caused by the increase in shear stress near the TCP. Thompson and Troian [13] studied slip at the wall with varying shear rates for a single phase fluid where they demonstrated a similar nonlinear behavior of slip length at high shear rates. From Fig. 4, it is seen that for the hydrophilic case, deviation from L_s^o occurs at about 10σ away from the TCP, where σ represents the diameter of the fluid molecules. In the case of a hydrophobic wall, the deviation starts at a distance of 30σ from the TCP. The length along which the deviation occurs appears to scale with the slip length. Since our circulation model assumes a constant slip length along the wall, the model breakdowns for droplets with lengths that are of the same order of magnitude as the slip length.

The second cause for error in the circulation model is significant for low $\mathcal{AR}$ droplets. The total circulation for low aspect ratio droplets is observed to deviate from the collapsed curve (Fig. 2(*b*)) and show significant error (Fig. 3). This is attributed to

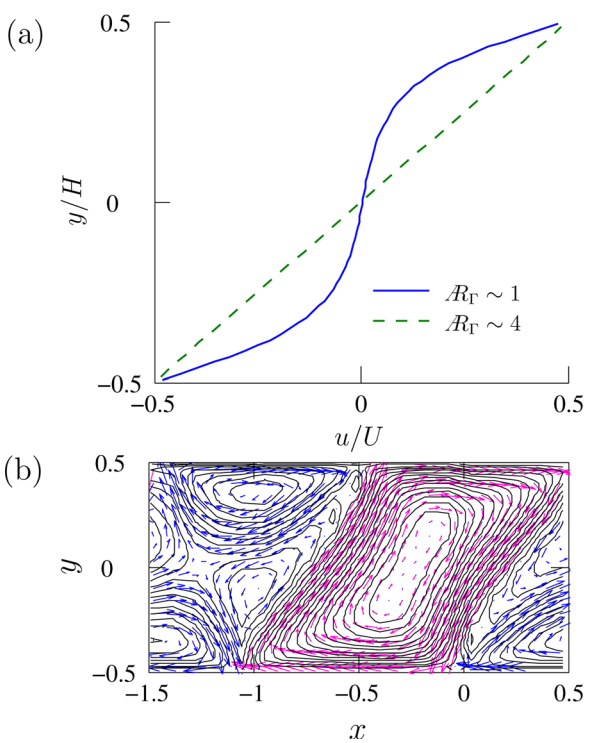

Fig. 5 (*a*) Axial velocity profile across the droplet center ($x/L = 0.5$) for $\mathcal{AR} = 1$ and 4. Droplet with $\mathcal{AR} = 4$ exhibits a linear velocity profile while for $\mathcal{AR} = 1$, deviation from the linear velocity profile of a Couette flow is seen which also suggests the formation of two circulatory flows in a droplet. (*b*) The velocity field for two droplets of $\mathcal{AR} = 1$ has a viscosity of $\mu_1 = 0.01\mu_2$, where μ_1 is the viscosity of the droplet on the left, and μ_2 is the viscosity of the droplet on the right. These results are for the case with no-slip at the wall.

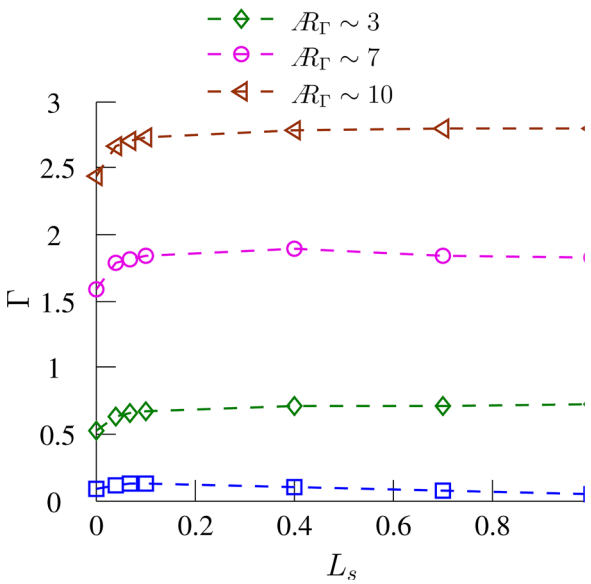

Fig. 6 Circulation versus slip length for droplets with different $\mathcal{AR}$. For the case of a Poiseuille flow, the aspect ratio of vortex is $\mathcal{AR}_\Gamma = 2\,\mathcal{AR}$.

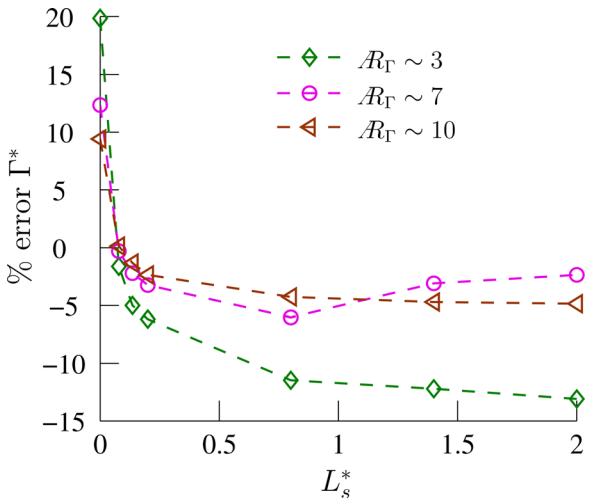

Fig. 7 Percentage error of nondimensional droplet circulation. The error is computed as $(\Gamma^*_{\text{model}} - \Gamma^*_{\text{simulation}})/\Gamma^*_{\text{simulation}}$, where $\Gamma^* = \Gamma/\tilde{U}L$. For the most part, the relative error is within 10%. The model breaks down for a $\mathcal{AR}_\Gamma = 1$ due to the deviation of its velocity profile from a single-phase Poiseuille flow.

the assumption of linear axial velocity profile, which is violated in a low $\mathcal{AR}$ droplet where the interface interference is evident at any axial location along the droplet. Figure 5(*a*) presents the axial velocity profile at the center of the droplet for two different aspect ratios. It is observed that the velocity profile for $\mathcal{AR} = 1$ deviates from the linear velocity profile in a Couette flow. This suggests the breakdown of the primary vortex into two separate vortices. Figure 5(*b*) shows two droplets of $\mathcal{AR} = 1$, having a viscosity of $\mu_1 = 0.01\mu_2$, where μ_1 is the viscosity of the droplet on the left, and μ_2 is the viscosity of the droplet on the right. The droplet with viscosity μ_1 has two distinct vortices, while the droplet with viscosity μ_2 has the primary vortex starting to breakdown. Hence, it can be inferred that viscosity, which can be considered as a measure of the extent of diffusion of momentum into a fluid, is also responsible for when the primary vortex breaks down. Since our circulation model is based on the assumption of having a linear velocity profile, deviation from this leads to the breakdown of the model and is a major cause of the increased error in circulation model.

5.2 Pressure/Body Force-Driven Flow. The circulation model for a droplet driven by a pressure/body force assumes a parabolic Poiseuille velocity profile. In a single phase Poiseuille flow, the presence of slip at the wall results in a velocity profile obtained by the superposition of a parabolic velocity profile with a uniform flow of velocity $4L_s/H$. Since uniform flow has no circulation, for a single phase flow, slip at the wall–fluid interface does not change the total circulation. Hence, the droplet circulation model in Eq. (18) is found to be independent of the slip length at the wall. This suggests that geometrically similar droplets could have similar total circulation no matter what the slip length is. As seen in Fig. 6, the total droplet circulation is primarily a constant for varying values of slip length. However, change in total circulation is observed from $L_s = 0$ to $L_s = 0.1$. This is because while in a force-driven single phase Poiseuille flow, the constant driving force is balanced by the shear force; for a droplet driven by a constant body force, the driving force is balanced by the capillary force in addition to the shear force. The capillary force is proportional to the mean curvature of the fluid–fluid interface, given by the Young–Laplace equation [26,27]. The mean curvature of an interface for a moving droplet is dependent on the capillary number and the wettability of the wall–fluid pair, given by the static contact angle or slip length [24]. Hence, the change in the capillary force due to slip at the wall results in the change in the characteristic velocity of the droplet, $\tilde{U}$. From the results presented, the relative change in total circulation due to change in capillary forces is less than 15% and is limited to small slip lengths. For the case of a body-driven flow, aspect ratio of the vortex is twice the droplet aspect ratio, $\mathcal{AR}_\Gamma = 2\mathcal{AR}$. The effect of droplet $\mathcal{AR}$ and the height of the droplet relative to slip length, on total circulation, are the same as that for a boundary-driven flow.

The accuracy of the circulation model in Eq. (18), developed in Sec. 4, is evaluated by comparing with simulation results; see Fig. 7. The relative error is plotted against slip length, for droplets with different aspect ratios, $\mathcal{AR}$, and viscosity ratio, μ_{12}. For the most part, the relative error is bounded to 10%. The three main sources of error can be traced back to the assumption of constant slip length along the wall, the assumption of parabolic Poiseuille velocity profile throughout the droplet, and the accuracy in predicting the characteristic velocity, $\tilde{U}$. The first two sources of error are similar to that of a boundary-driven flow which was discussed in Sec. 5.1. The third source of error is associated with the prediction of characteristic velocity, which is discussed below.

The effective pressure gradient experienced by the droplet is determined by the magnitude of the pressure drop, at points inside the droplets adjacent to the two interfaces, divided by the distance separating them. Hence, as mentioned previously (Sec. 4), the change in total force acting on the droplet caused by the capillary pressure is inversely proportional to the droplet $\mathcal{AR}$. This is observed by comparing the velocity profile at the center of the droplet, for different aspect ratios, to that of the single phase Poiseuille profile; see Fig. 8. The droplet velocity profile approaches that of the single phase Poiseuille profile as the droplet $\mathcal{AR}$ increases. It is seen that similar to the boundary-driven flows, the velocity profile for low droplet aspect ratios deviates from the parabolic profile of a Poiseuille flow due to the close proximity of the two fluid–fluid interface. Several models are presented in the literature that predicts the effective pressure gradient across a droplet or the characteristic velocity of the droplet, $\tilde{U}$ [25]. In this paper, the model presented in Eq. (17) is used to predict the characteristic velocity of the droplet, which accounts for change in effective pressure gradient due to capillary pressure. The details of the model were presented in Sec. 4. Droplet circulation, scaled by $\tilde{U}L$, is plotted against slip length, scaled by H, in Fig. 9. The data for different droplet aspect ratios and for a slip length of $L_s = 0$ collapse, except for $\mathcal{AR} = 1$, showing that the model

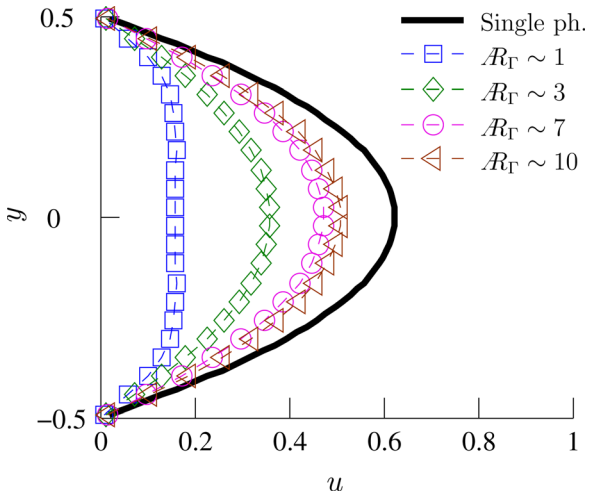

Fig. 8 Axial velocity profile at the droplet center ($x/L = 0.5$) for different droplet aspect ratios. Velocity profile for single phase Poiseuille flow is shown in solid line.

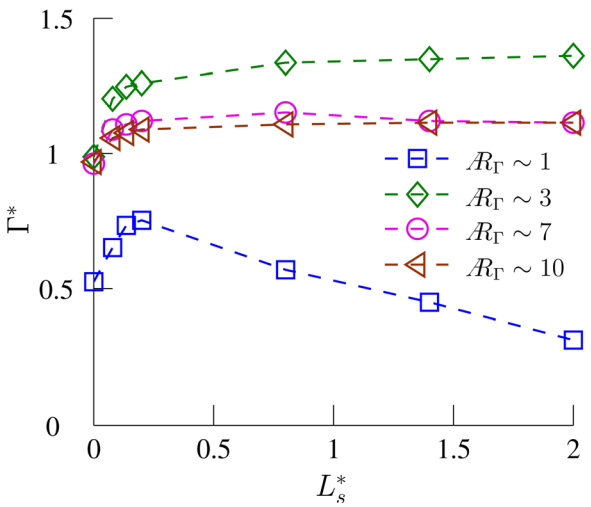

Fig. 9 Scaled droplet circulation is plotted against the nondimensional slip length, where $\Gamma^* = \Gamma/UL$ and $L_s^* = L_s/(H/2)$

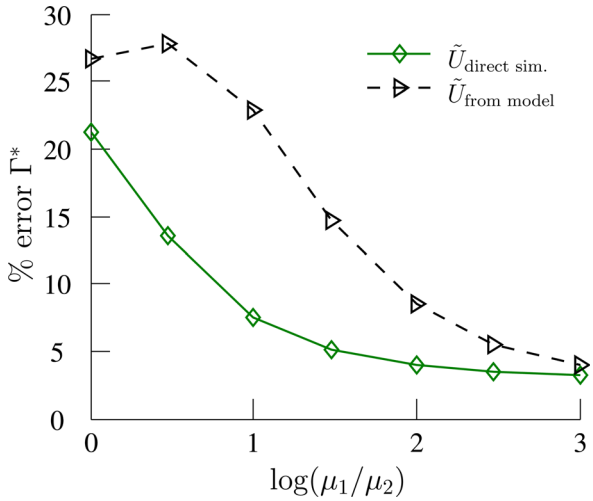

Fig. 10 Percentage error of nondimensional droplet circulation versus viscosity ratio, where centerline velocity is (*a*) directly obtained from simulation, $\tilde{U}_{\text{direct sim.}}$, and (*b*) predicted using model presented in Eq. (17) $\tilde{U}^*_{\text{from model}}$

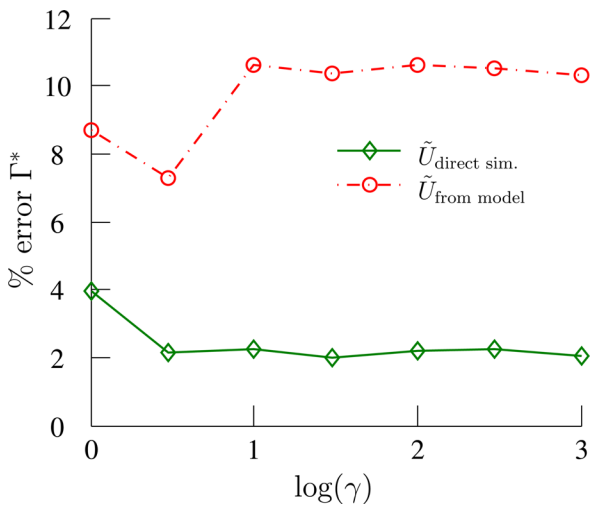

Fig. 11 Percentage error of nondimensional droplet circulation versus interfacial tension, where centerline velocity is (*a*) directly obtained from simulation, $\tilde{U}_{\text{direct sim.}}$, and (*b*) predicted using model presented in Eq. (17) $\tilde{U}^*_{\text{from model}}$

presented by Eq. (17) captures the effect of the capillary pressure for varying droplet aspect ratios correctly. The scaling for circulation is consistent with the experimental results of Ref. [20], for the limiting case of no-slip ($L_s = 0$) at the wall. Results for cases of slip length not corresponding to no-slip boundary condition do not collapse as the model does not account for the effect of slip length on capillary force. The model is verified for varying viscosity ratios and interfacial tensions. In Fig. 10, we plot the error in estimating nondimensional circulation over a large range of viscosity ratios. It is seen that when the centerline velocity from the simulation is used to scale the total circulation in a droplet, the error of prediction of the circulation model is within 10% for droplets with $\mu_1/\mu_2 \geq 10$ and increases to 20% for viscosity ratios smaller than that. Using the centerline velocity as given by Eq. (17) gives similar results, with error less than 10% for high viscosity ratios. Here, the numerical coefficient, A, is evaluated for $\mu_1 = \mu_2$. Many of the commonly used fluid pairs have high viscosity ratios, for example, water–air or castor oil–water has a viscosity ratio of $\approx$100 and $\approx$1000, respectively. Hence, it can be concluded that the circulation model provides a good estimation for circulation over a wide range of viscosity ratios and that the scaling is correct. Similar to the viscosity ratio, we plot the error in estimating nondimensional circulation for different values of interfacial tensions, as shown in Fig. 11. When the centerline velocity from the simulation is used to scale the total circulation in the droplet, it is seen that the error of prediction of the circulation model is less than 10%. This is also the case when circulation is scaled using the centerline velocity estimated by Eq. (17). Here, the numerical coefficient, A, is evaluated for $\gamma = 1$. Hence, as before, the circulation model and the scaling are valid for a wide range of interfacial tension values. A note should be made that Eq. (17) was for a single droplet in a channel. In the case of multiple droplets in a channel, the net effect of capillary force needs to be scaled by the number of droplets [25].

In the cases considered in this paper, the static contact angle was assumed to be a constant, equal to 90 deg, for varying degrees of slip at the wall–fluid interface. This is because, in order to find static contact angle corresponding to different values of slip length, separate experiments need to be performed. As previously discussed, for droplet with large $\mathcal{A}R$, the centerline and wall are the primary contributors to the total circulation. Hence, being able to predict the characteristic velocity of the droplet is essential for increasing the accuracy of the model.

5.3 Effect of Slip at the Fluid–Fluid Interface on Droplet Circulation. In the current study, only the case of immiscible fluids was considered but a fluid–fluid interface of a droplet, in general, could also be partially miscible. Koplik and Banavar [32] had shown that slip at the fluid–fluid interface is analogous to the Navier slip model. Immiscible fluids have a sharp, distinct interface where the two fluids do not experience any transfer of tangential momentum at the interface. This is analogous to a fluid with perfect slip at the wall. In the case of partially miscible fluids, the interaction between the two fluids leads to a change in momentum along the interface. As the vortex in the droplet and the fluid surrounding it are corotating, there could be an apparent reduction in the total circulation in a droplet, depending on the relative molecular mass of the two fluids. But, as circulation is calculated over a material line, the occurrence of mass transfer across the interface leads to difficulties in its calculation.

6 Conclusion

Circulation is an important factor that affects mixing, heat transfer, and chemical reaction inside a droplet, which have many practical applications. Hence, a change in circulation directly impacts the rate of mixing, mass and heat transfer, and chemical reaction, essential for various droplet-based microfluidic devices. A simple theoretical model is developed where the droplet circulation could be predicted from the a priori known quantities about the droplet, it shows the dependence of circulation on slip length and droplet $\mathcal{AR}$. The model demonstrates that for a boundary-driven flow, circulation in a droplet decreases with increasing slip length, while for a body force-driven flow it is primarily independent of slip length. For a 2D boundary-driven flow, the droplet circulation model is given as

$$\frac{\Gamma}{UL} = \frac{2}{1 + 2\dfrac{L_s}{H}}\left(1 + \frac{k}{\mathcal{AR}_\Gamma \sin\theta}\right)$$

where Γ is the droplet circulation, U is the centerline velocity of the droplet, L is the length of the droplet, H is the height of the droplet, L_s is the slip length of the wall–fluid pair, $\mathcal{AR}_\Gamma$ is the aspect ratio of the vortex, and k is a fixed coefficient. Droplet circulation model for a 2D pressure/body force-driven flow is

$$\frac{\Gamma}{\tilde{U}L} = 1 + \frac{2k}{\mathcal{AR}_\Gamma \sin\theta}$$

It helps to identify the scaling parameters for circulation and slip length. The model is validated using results from continuum simulations. Effect of slip at the fluid–fluid interface on circulation is also briefly discussed.

Acknowledgment

This research was supported by the Office of Naval Research.

References

[1] Reyes, D. R., Iossifidis, D., Auroux, P.-A., and Manz, A., 2002, "Micro Total Analysis Systems. 1. Introduction, Theory, and Technology," Anal. Chem., **74**(12), pp. 2623–2636.
[2] Auroux, P.-A., Iossifidis, D., Reyes, D. R., and Manz, A., 2002, "Micro Total Analysis Systems. 2. Analytical Standard Operations and Applications," Anal. Chem., **74**(12), pp. 2637–2652.
[3] Koh, W. H., Lok, K. S., and Nguyen, N. T., 2013, "A Digital Micro Magneto-fluidic Platform for Lab-on-a-Chip Applications," ASME J. Fluids Eng., **135**(2), p. 021302.
[4] Burns, J., and Ramshaw, C., 2001, "The Intensification of Rapid Reactions in Multiphase Systems Using Slug Flow in Capillaries," Lab Chip, **1**(1), pp. 10–15.
[5] Dummann, G., Quittmann, U., Gröschel, L., Agar, D. W., Wörz, O., and Morgenschweis, K., 2003, "The Capillary-Microreactor: A New Reactor Concept for the Intensification of Heat and Mass Transfer in Liquid–Liquid Reactions," Catal. Today, **79–80**, pp. 433–439.
[6] Jaritsch, D., Holbach, A., and Kochmann, N., 2014, "Counter-Current Extraction in Microchannel Flow: Current Status and Perspectives," ASME J. Fluids Eng., **136**(9), p. 091211.
[7] Mohseni, K., 2005, "Effective Cooling of Integrated Circuits Using Liquid Alloy Electrowetting," Semiconductor Thermal Measurement, Modeling, and Management Symposium (SEMI-Therm), IEEE, San Jose, CA, Mar. 15–17, pp. 20–25.
[8] Baird, E., and Mohseni, K., 2008, "Digitized Heat Transfer: A New Paradigm for Thermal Management of Compact Micro-Systems," IEEE Trans. Compon. Packag. Technol., **31**(1), pp. 143–151.
[9] Hosokawa, K., Fujii, T., and Endo, I., 1999, "Handling of Picoliter Liquid Samples in a Poly(dimethylsiloxane)-Based Microfluidic Device," Anal. Chem., **71**(20), pp. 4781–4785.
[10] Song, H., Tice, J. D., and Ismagilov, R. F., 2003, "A Microfluidic System for Controlling Reaction Networks in Time," Angew. Chem. Int. Ed., **42**(7), pp. 768–772.
[11] Navier, C., 1823, "Memoire sur les lois du mouvement des fluides," Mem. Acad. R. Sci. Inst. Fr., **6**, pp. 389–440.
[12] Maxwell, J., 1890, *The Scientific Papers of James Clerk Maxwell*, Vol. V2, Cambridge University Press, Cambridge, pp. 703–711.
[13] Thompson, P., and Troian, S., 1997, "A General Boundary Condition for Liquid Flow at Solid Surfaces," Nature, **389**, pp. 360–362.
[14] Thalakkottor, J., and Mohseni, K., 2013, "Analysis of Slip in a Flow With an Oscillating Wall," Phys. Rev. E, **87**, p. 033018.
[15] Koplik, J., and Banavar, J., 1995, "Continuum Deductions From Molecular Hydrodynamics," Annu. Rev. Fluid Mech., **27**, pp. 257–292.
[16] Koplik, J., Banavar, J., and Willemsen, J., 1989, "Molecular Dynamics of Fluid Flow at Solid Surfaces," Phys. Fluids A, **1**(5), pp. 781–794.
[17] Koplik, J., Banavar, J., and Willemsen, J., 1988, "Molecular Dynamics of Poiseuille Flow and Moving Contact Lines," Phys. Rev. Lett., **60**(13), pp. 1282–1285.
[18] Thompson, P., and Robbins, M., 1989, "Simulations of Contact Line Motion: Slip and the Dynamic Contact Angle," Phys. Rev. Lett., **63**, pp. 766–769.
[19] Paik, P., Pamula, V. K., and Fair, R. B., 2003, "Rapid Droplet Mixers for Digital Microfluidic Systems," Lab Chip, **3**(2), pp. 253–259.
[20] DeVoria, A. C., and Mohseni, K., 2005, "Droplets in an Axisymmetric Microtube: Effects of Aspect Ratio and Fluid Interfaces," Phys. Fluids, **27**(1), pp. 80–101.
[21] Taheri, P., Torrilhon, M., and Struchtrup, H., 2009, "Couette and Poiseuille Microflows: Analytical Solutions for Regularized 13-Moment Equations," Phys. Fluids, **21**(1), p. 017102.
[22] Popinet, S., 2009, "An Accurate Adaptive Solver for Surface-Tension-Driven Interfacial Flow," J. Comput. Phys., **228**(16), pp. 5838–5866.
[23] Plimpton, S., 1995, "Fast Parallel Algorithms for Short-Range Molecular Dynamics," J. Comput. Phys., **117**(1), pp. 1–19.
[24] Kistler, S. F., 1993, *Wettability*, J. C. Berg, ed., Marcel Dekker, New York.
[25] Baroud, C. N., Gallaire, F., and Dangla, R., 2010, "Dynamics of Microfluidic Droplets," Lab Chip, **10**(16), pp. 2032–2045.
[26] Young, T., 1805, "An Essay on the Cohesion of Fluids," Philos. Trans. R. Soc. London, **95**, pp. 65–87.
[27] Laplace, P., 1805, *Traité de mécanique céleste/par, PS Laplace, tome quatrieme*, Vol. 4, de l'Imprimerie de Crapelet, Paris.
[28] Fuerstman, M. J., Lai, A., Thurlow, E., Shevkoplyas, S. S., Stone, H. A., and Whitesides, G. M., 2007, "The Pressure Drop Along Rectangular Microchannel Containing Bubbles," Lab Chip, **7**(11), pp. 1479–1489.
[29] Mohseni, K., and Baird, E., 2007, "A Unified Velocity Model for Digital Microfluidics," Nanoscale Microscale Thermophys. Eng., **11**(1–2), pp. 109–120.
[30] Ou, J., Perot, B., and Rothstein, J. P., 2004, "Laminar Drag Reduction in Microchannels Using Ultrahydrophobic Surfaces," Phys. Fluids, **16**(12), pp. 4635–4643.
[31] Choi, C. H., and Kim, C. J., 2006, "Large Slip of Aqueous Liquid Flow Over a Nanoengineered Superhydrophobic Surface," Phys. Rev. Lett., **96**(6), p. 066001.
[32] Koplik, J., and Banavar, J. R., 2006, "Slip, Immiscibility, and Boundary Conditions at the Liquid–Liquid Interface," Phys. Rev. Lett., **96**(4), p. 044505.